**PAPER** • **OPEN ACCESS**

# Lattice-matched III-nitride structures comprising BAlN, BGaN, and AlGaN for ultraviolet applications

To cite this article: Feras AlQatari *et al* 2021 *Mater. Res. Express* **8** 086202



Materials Research Express

PAPER

# Lattice-matched III-nitride structures comprising BAlN, BGaN, and AlGaN for ultraviolet applications

**Feras AlQatari**[1], **Muhammad Sajjad**[2], **Ronghui Lin**[1], **Kuang-Hui Li**[1], **Udo Schwingenschlögl**[2] and **Xiaohang Li**[1]

[1] Advanced Semiconductor Laboratory, King Abdullah University of Science and Technology (KAUST), Thuwal 23955-6900, Saudi Arabia
[2] Physical Science and Engineering Division, King Abdullah University of Science and Technology (KAUST), Thuwal 23955-6900, Saudi Arabia

**E-mail:** xiaohang.li@kaust.edu.sa

**Keywords:** BAlN, BGaN, refractive index, absorption index, strain-free DBR

Supplementary material for this article is available online

OPEN ACCESS

RECEIVED
22 May 2021

REVISED
2 August 2021

ACCEPTED FOR PUBLICATION
11 August 2021

PUBLISHED
18 August 2021



## Abstract

The optical properties of BAlN, BGaN and AlGaN ternary alloys are investigated using hybrid density functional for the design of lattice-matched optical structures in the ultraviolet spectrum. The calculated AlGaN properties agree well with previous reports, validating the model. A peculiar non-monotonic behavior of the refractive index as a function of the boron composition is found. The results of this calculation are interpolated to generate a three-dimensional dataset, which can be employed for designing a countless number of lattice-matched and –mismatched heterostructures. These heterostructures could span a range of operating wavelengths well into the deep ultraviolet with refractive indices ranging from 1.98 to 2.41 for AlN at 0 eV and GaN near the GaN bandgap, respectively. An example is shown where a lattice-matched heterostructure, AlN/$B_{0.108}Ga_{0.892}N$, is applied for DBR applications with a large index difference. A DBR comprising the AlN/$B_{0.108}Ga_{0.892}N$ heterostructure at the UV wavelength of 375 nm is found to exceed 93% peak reflectivity with only 10 pairs and reaches 100% reflectivity with 35 pairs. For a chosen design with 25 pairs, the DBR has a peak reflectivity of 99.8% and a bandwidth of 26 nm fulfilling the requirements of most devices especially ultraviolet vertical-cavity surface emitting lasers.

## 1. Introduction

Wurtzite III-nitride semiconductor materials have many technically important properties for applications in optical and electronic devices [1]. The III-nitride based optical devices can operate over a wide spectrum of wavelengths from infrared (IR) to ultraviolet (UV) [2] due to highly tunable bandgaps from ~0.7 to ~6 eV [3]. The interests in developing UV devices such as UV light-emitting diodes (LEDs), photodetectors, and lasers are rapidly rising for vital applications such as sterilization, data storage, biochemical sensing, atomic clocks, and communication [4–14].

Optical structures such as distributed Bragg reflectors (DBRs) are essential in UV surface-emitting lasers for cavity formation and UV LEDs for higher light extraction efficiency [15–17]. DBRs are dielectric or semiconducting superlattices capable of achieving up to 100% reflectivity. However, the formation of cracks and compromised crystal quality due to strain and lattice mismatch can greatly harm a DBR's performance [18]. Thus, both lattice matching and large refractive index contrast are desirable especially for epitaxial DBRs. In the past, AlGaN-based heterojunctions, including $Al_xGa_{1-x}N/Al_yGa_{1-y}N$ superlattices, have been used for various UV applications where the higher index contrast leads to higher lattice mismatch [19–21]. In theory, InAlN would be suitable for lattice matching with AlGaN alloys, though it could be challenging to grow high quality InAlN with large indium composition due to large atomic size difference, phase separation, and epitaxial temperature incompatibility between InN (~600 °C) and AlN (⩾1100 °C) [22, 23]. This leads to relatively complex growth methods for the realization of near lattice-matched AlGaN/InAlN DBR [24].

Recently, the search for materials suitable for more UV and power devices in the wurtzite III-nitride system has inspired a number of studies of boron-containing III-nitrides including BAlN and BGaN[18, 25–35]. Alloying III-nitrides with boron can reduce their lattice parameters giving a new option for strain engineering and lattice matching [36]. In addition, the incorporation of boron could lead to more alloys with larger bandgaps than that of GaN, adding more options for device engineering.

The refractive index is critical for the design and simulation of optoelectronic devices in the UV range. It has been experimentally shown that a small incorporation of boron into GaN and AlN can cause a significant change in the refractive index of materials [25, 26]. Recently, the full range of compositions of BGaN alloys has been investigated by Said *et al* using the local density approximation of density functional theory [28]. Additionally, Yamashita *et al* have studied wurtzite $B_xAl_{1-x}N$ with low boron compositions ($x \leqslant 0.5$) also using the local density approximation [37]. However, it is well known that such local functionals could severely underestimate the bandgaps, redshift absorption spectra, miss excitonic features in dielectric function, and have a tendency to overestimate the static dielectric function as Paier *et al* have shown [38]. This this an issue because the refractive index is an electronic-band-structure dependent property and most models assume an inverse correlation of the index with bandgap (see supporting information). In comparison, the use of hybrid functionals gives much more reliable results. This led both Said *et al* and Yamashita *et al* to employ a rigid shift of the conduction band to compensate for the limitations of the local density approximation.

In this work, we performed computations of the lattice parameters and the refractive indices of the $B_xAl_{1-x}N$ and $B_xGa_{1-x}N$ alloys ($0 \leqslant x \leqslant 1$). The index calculation of the $Al_xGa_{1-x}N$ alloys ($0 \leqslant x \leqslant 1$) was carried out to compare with the reports of the extensively studied $Al_xGa_{1-x}N$ alloys for validating the calculation methodology [39, 40]. Hybrid density functional theory was employed for an accurate calculation of the optical properties. Furthermore, the refractive indices of the three ternary alloys and the lattice constants were employed to identify lattice-matched material pairs with a large index difference for DBR applications.

## 2. Computational details

The calculations were carried out using the Vienna *Ab initio* Simulation Package [41, 42]. Before calculating the indices, the wurtzite structures of the alloys were optimized using the general gradient approximation (GGA-PBEsol) of the exchange-correlation potential [43]. The energy cutoff was set to 520 eV for the plane-wave basis set. The structure optimization was performed on primitive cells for the binary materials, i.e. BN, AlN, and GaN; and on 16-atom supercells for the ternary $A_xC_{1-x}N$ alloys (A = B, Al; C = Al, Ga; $0 \leqslant x \leqslant 1$) with chalchopyrite-like (CH) and luzonite-like (LZ) structures for $x = 0.5$, and 0.25 and 0.75, respectively [29]. In addition, the calculation was performed for $B_xAl_{1-x}N$ and $B_xGa_{1-x}N$ alloys with $x = 0.125$, representing the alloys with lower boron compositions, closer to experimental works [18, 30, 31, 35, 36]. For these two alloys, we utilized the same LZ structure as $x = 0.25$, but with the replacement of one boron atom with an aluminum or a gallium atom. All structures were relaxed until Hellman–Feynman forces reached less than 0.02 eVÅ$^{-1}$. The Γ-centered k-mesh was set to $6 \times 6 \times 6$ for the structural optimizations. Figure 1 shows the calculated lattice parameters of the $Al_xGa_{1-x}N$, $B_xAl_{1-x}N$ and $B_xGa_{1-x}N$ alloys ($0 \leqslant x \leqslant 1$), where the results of binaries and ternaries show good agreement with reported experimental and theoretical discoveries [29, 44].

To calculate the optical properties, the hybrid functional of Heyd, Scuseria, and Ernzerhof (HSE) [45] was employed using the optimized lattice structures assuming the light polarization is perpendicular to the *c*-axis. Similar to the structure optimization, 520 eV was utilized as the energy cutoff for the plane-wave basis set. Γ-centered k-meshes of $8 \times 8 \times 8$ and $6 \times 6 \times 6$ were adopted for the binaries and ternaries, respectively. The number of bands was converged for optical properties, and 96 bands were used for all cells. The same parameters were used for the AlGaN, BAlN, and BGaN alloys.

## 3. Results and discussion

The refractive and absorption indices of AlGaN alloys, shown in figures 2(a) and (b), have a monotonic trend where both the index and its slope increase as the Ga content is increased (Al is decreased). Figures 2(c) and (d) compare our results with experimental results measured at room temperature, showing similar trends and degrees of dispersion (slope of refractive index versus energy) [39, 40]. Our model underestimates the refractive index by a small percentage between 0 and 6.5% depending on composition, which is a smaller error than found by other methods [46, 47]. Additionally, this error may be related to the temperature dependence of the refractive index which is not accounted for in our model as density functional theory does not account for temperature by default [48, 49].

The calculated values for boron alloys are reported in figure 3. Both absorption and refractive indices are calculated using the complex dielectric function (supporting information) as described in the following

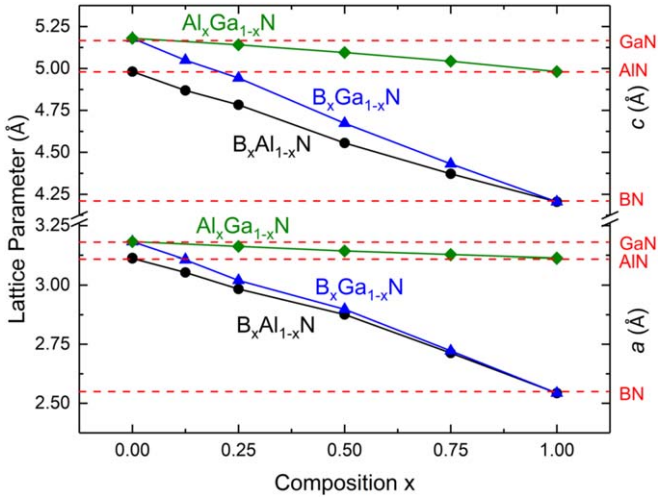


**Figure 1.** Calculated lattice parameters *a* and *c* of different wurtzite $A_xC_{1-x}N$ alloys (A = B, Al; C = Al, Ga; $0 \leqslant x \leqslant 1$) compared to those of the binary wurtzite materials from [44] (marked by the dashed red lines).

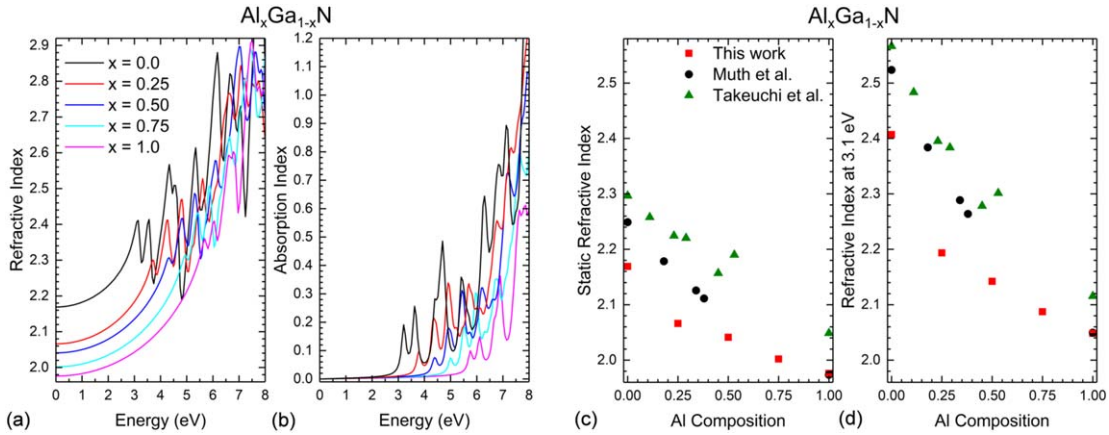


**Figure 2.** The calculated (a) refractive indices and (b) absorption indices of the $Al_xGa_{1-x}N$ alloys. (c) and (d) Comparison of the refractive index of $Al_xGa_{1-x}N$ obtained in this study and reported by Muth *et al* [40] and Takeuchi *et al* [39] through experimental works: (c) Static refractive index at 0 eV and (d) refractive index at 3.1 eV right below the GaN bandgap.

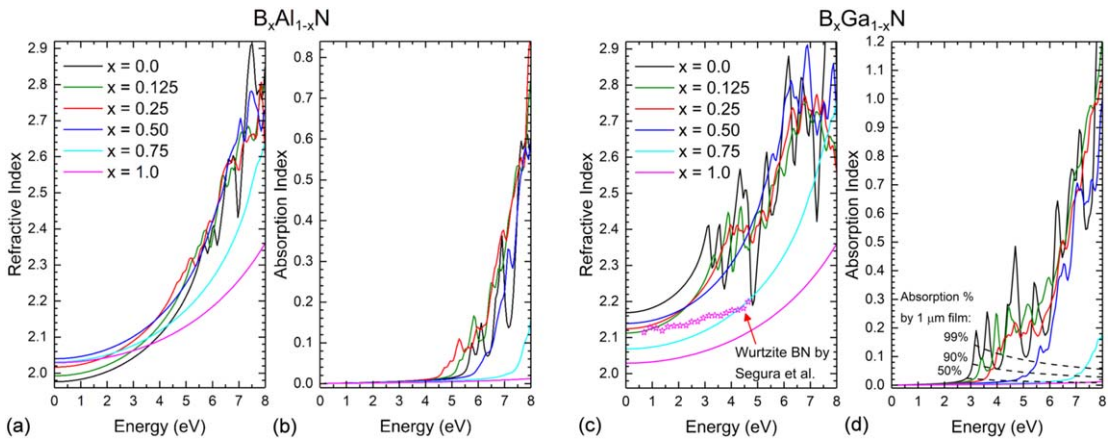


**Figure 3.** Refractive and absorption indices of the $B_xAl_{1-x}N$ (a) and (b) and $B_xGa_{1-x}N$ (c) and (d) alloys as a function of photon energy. The dashed lines in (d) show the curves for different absorption percentages when light goes through a 1 $\mu$m film (supporting information). The magenta stars in (c) show the refractive indices of BN as measured by Segura *et al* for comparison [51].

definition [50]:

$$n = \frac{1}{\sqrt{2}}\sqrt{\sqrt{{\varepsilon_1}^2 + {\varepsilon_2}^2} + \varepsilon_1},$$

and

$$\kappa = \frac{1}{\sqrt{2}}\sqrt{\sqrt{{\varepsilon_1}^2 + {\varepsilon_2}^2} - \varepsilon_1} \quad (1)$$

$n$ is the refractive index, $\kappa$ is the absorption index, and $\varepsilon_1$ and $\varepsilon_2$ are the real and imaginary parts of the dielectric function, respectively.

Figure 3 shows the refractive and absorption indices of the BAlN and BGaN alloys. The refractive indices exhibit positive slopes; and the absorption indices stay close to zero then rise when approaching the respective optical bandgaps [34, 52]. This is similar to other wurtzite nitrides such as AlGaN and InGaN. However, another trend is observed when considering compositions where the refractive indices below the bandgaps of BAlN and BGaN do not always decrease with reduced lattice parameters. See supporting information for an in depth discussion.

It is important to compare our results with the few experimental works investigating the optical properties of wurtzite BN and its alloys. Recently, Segura *et al* measured the refractive index of wurtzite BN at the UV-visible range [51]. The magenta stars in figure 3(c) show the comparison between Segura's and our index values. It is remarkable to see that the difference between the two is less than ~5%, and that the slope in our result is similar to the experimental value for BN at the energy range 1–5 eV [51].

Other earlier experimental works exploring the refractive indices of low boron composition BAlN and BGaN show trends that are different from each other and from our results [25, 26, 53, 54]. See supporting information for a detailed comparison. We believe that the apparent disagreement for both BGaN and BAlN between some experimental results with our calculations is likely the result of factors other than boron composition causing a larger decrease in index in their results. Low (wurtzite) crystallinity and high levels of impurity such as carbon may both be at play amongst other unknown issues [55, 56]. Additionally, the characterization technique used to estimate the boron composition was not reported by Watanabe; and neither Gautier nor Watanabe reported on possible impurities and their levels; thus the results may not be directly comparable to each other nor to ours [26, 54].

To design III-nitride optical structures including DBRs for UV applications, it is imperative to consider multiple factors simultaneously, including the target wavelength range, the lattice parameters, and the refractive index. The lattice parameters as a function of the composition (figure 1) and the refractive indices as a function of wavelength (figures 2 and 3) of the $Al_xGa_{1-x}N$, $B_xAl_{1-x}N$, and $B_xGa_{1-x}N$ alloys ($0 \leqslant x \leqslant 1$) were correlated and two-dimensional (2D)-interpolated using the Modified Akima cubic Hermite method [57]. This interpolation method was chosen due to its lower variations in the predicted variable than when using the spline interpolation method [58]. Additionally, it has less sharp edges when compared to linear interpolation. This, we believe, would give a more sensible prediction of refractive index curves with a high compositional resolution. Subsequently, they were plotted in a three-dimensional (3D) chart shown in figure 4 for the design of optically-transparent UV DBR pairs.

Based on the 3D chart in figure 4, one can identify a virtually infinite number of lattice-matched material pairs with various refractive index differences important for minimized structural thickness and for strain management. Additionally, one can name numerous material pairs with certain lattice mismatch levels for device strain engineering while accommodating the need for maintaining certain index differences for different applications [59, 60].

For instance, the index difference $\Delta n$ between two lattice-matched and optically-transparent alloys as a function of the lattice parameter and the wavelength can be extracted from figure 4, as shown in figure 5(a). From figure 5(a), the overall largest index difference is formed between AlN and $B_{0.108}Ga_{0.892}N$ with the same lattice constant of 3.113 Å, ranging from 0.14 to 0.27 at 370 (UVA)−1500 (IRB) nm. In general, the index difference narrows when the lattice parameter shifts away from that of AlN towards those of GaN and BN.

Subsequently, the knowledge of the refractive index of lattice-matched material pairs can be utilized to compute the theoretical bandwidth $\Delta\lambda$ of the material pair at various wavelengths for the DBR according to equation (2) where $\lambda_0$ is the design wavelength, $\rho$ is reflection coefficient, $n_H$ and $n_L$ are high and low refractive indices, respectively [61]. The results are shown in figure 5(b). The overall largest bandwidth values are 26−65 nm at the wavelength range 370−1500 nm which is found for the same $AlN/B_{0.108}Ga_{0.892}N$ pair due to it having the largest index difference. Note that the bandwidth gradually reduces as the wavelength is reduced, which is the reason behind the difficulty of designing a large bandwidth DBR for the UV range.

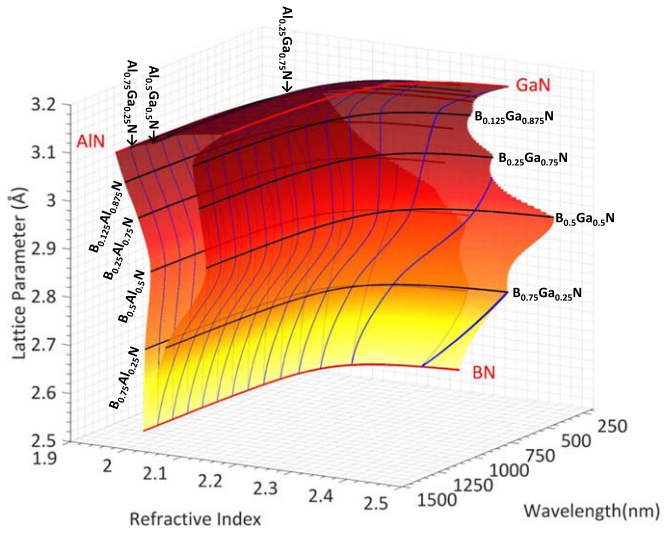


**Figure 4.** The 3D chart of the refractive indices of the $Al_xGa_{1-x}N$, $B_xAl_{1-x}N$, and $B_xGa_{1-x}N$ alloys ($0 \leqslant x \leqslant 1$) as a function of the photon wavelength (175–1500 nm) and the lattice parameter (2.5–3.2 Å) for the design of lattice-matched UV DBR pairs. The horizontal black curves represent the refractive indices of particular alloy compositions that we directly calculated using density functional theory. The three surfaces connecting the horizontal black (and red) curves are interpolated to show the expected indices of other compositions of the three alloys. The vertical blue curves represent borders of 100 nm thick slices based on the wavelength axis. Any two alloys with the same color have the same lattice parameter. The 3D chart is cut off when the $B_xGa_{1-x}N$ absorption is near 90% for a 1 $\mu$m thick film since $B_xGa_{1-x}N$ is always the lower bandgap material for any lattice matached pair comprising BGaN/AlGaN or BGaN/BAlN heterostrucutres (see figure 1 and dashed lines in figure 3). Therefore, the 3D chart applies for optically-transparent (or semitransparent) scenarios only.

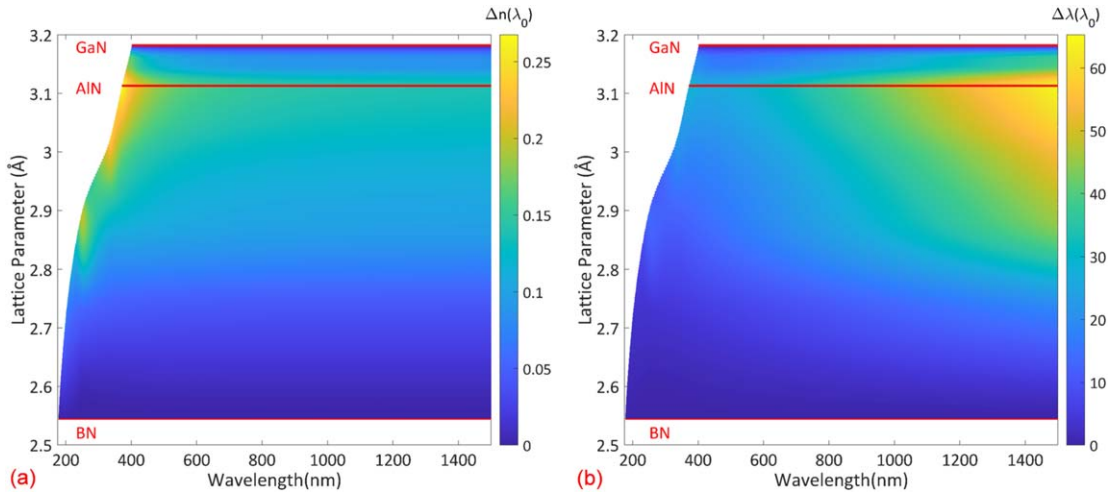


**Figure 5.** (a) The refractive index difference $\Delta n$ and (b) the theoretical DBR bandwidth $\Delta\lambda$ of lattice-matched material pairs as a function of the lattice parameter and the wavelength extracted from figure 4. The horizontal red lines indicate the lattice parameters of binary BN, AlN, and GaN as reference.

$$\Delta\lambda = \frac{\pi}{2}\lambda_0\left[\frac{1}{\arccos(\rho)}\frac{1}{\arccos(-\rho)}\right],$$

where

$$\rho = \frac{\Delta n}{n_H + n_L} = \frac{n_H - n_L}{n_H + n_L} \tag{2}$$

Finally, the AlN/$B_{0.108}Ga_{0.892}N$ pair was employed to simulate the performances of a few DBRs at a UVA wavelength of 375 nm. Accordingly, the thickness of the AlN and $B_{0.108}Ga_{0.892}N$ layers are 45.5 and 40.2 nm, respectively, based on their refractive indices of 2.06 and 2.33 at 375 nm. This wavelength is chosen partially due to recent interests in developing the UVA vertical-cavity surface-emitting lasers (VCSELs) near 375 nm for important applications including the atomic clock [14, 62–65]. The simulation was conducted by Lumerical

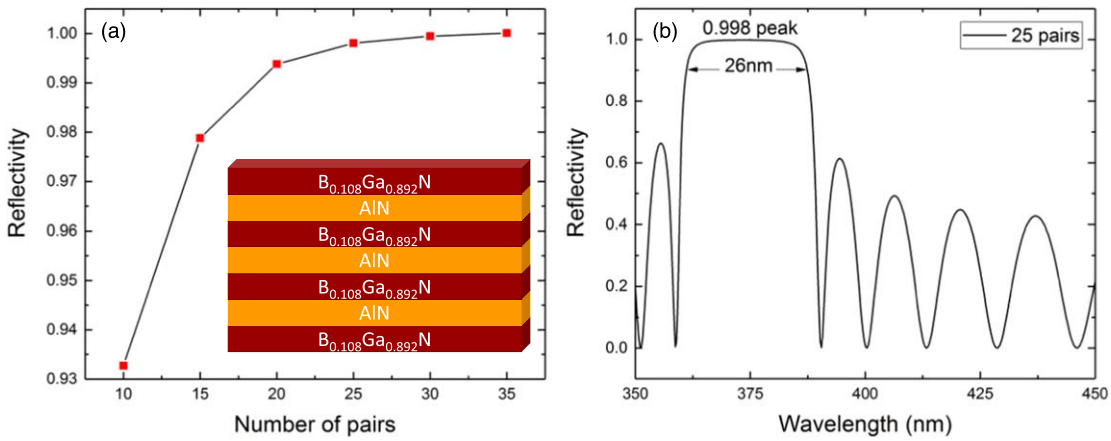


**Figure 6.** (a) DBR peak reflectivity as a function of the number of the lattice-matched AlN/$B_{0.108}Ga_{0.892}N$ pairs at 375 nm and (b) reflectivity as a function of wavelength for the 25-pair AlN/$B_{0.108}Ga_{0.892}N$ DBR. The inset of (a) shows a 3-pair DBR as an example.

**Table 1.** Performance comparison of different DBR structures for UVA applications. The bandwidth is taken at 90% of the peak reflectivity.

| Result type | Structure | Lattice mismatch | $\lambda_0$ (nm) | Pairs | Reflectivity | $\Delta\lambda$ (nm) | $\Delta$n |
|---|---|---|---|---|---|---|---|
| This work | $B_{0.108}Ga_{0.892}N$/AlN | 0% | 375 | 10 | 0.933 | 26 | 0.27 |
| | | | | 25 | 0.998 | | |
| Experiment [24] | $Al_{0.83}In_{0.17}N/Al_{0.2}Ga_{0.8}N$ | 0.511% | 368 | 45 | 0.993 | 13 | N/A |
| Experiment [19] | $Al_{0.12}Ga_{0.88}N$/GaN | 0.265% | 368 | 40 | 0.916 | 4.4 | 0.12 |
| Simulation [19] | | | 369 | 40 | 0.972 | 5.6 | |
| Experiment [20] | $Al_{0.18}Ga_{0.82}N/Al_{0.8}Ga_{0.2}N$ | 1.37% | 347 | 20 | 0.93 | 18 | 0.22 |
| | | | 347 | 25 | 0.99 | 22 | |
| Experiment [21] | $Al_{0.2}Ga_{0.8}N$/GaN | 0.436% | 380 | 60 | 0.99 | 8 | 0.17 |

FDTD Solutions [66]. The assumption of no optical absorption was made since 375 nm is below the bandgaps of AlN and $B_{0.108}Ga_{0.892}N$ (figure 3(d)) [52].

We started this simulation by sweeping different numbers of pairs to see the change in the peak reflectivity. Figure 6(a) indicates that the peak reflectivity reaches over 93% with only 10 pairs, exceeds 99% at 20 pairs, and plateaus after 25 pairs. The reflectivity spectrum of the 25-pair DBR is shown in figure 6(b), where the peak reflectivity is 99.8%. The bandwidth measured at 90% reflectivity is 26 nm as indicated by the arrow in figure 6(b).

Table 1 shows the comparison of the 10-pair and the 25-pair AlN/$B_{0.108}Ga_{0.892}N$ DBRs with a few reported DBRs designed for UVA applications, indicating superior properties of our proposed DBR which include no lattice mismatch, smaller number of pairs, higher reflectivity, and larger bandwidth. It is important to note that the results of this study can be extended to numerous other material pairs for lattice-matching or lattice-engineering needs at various wavelengths. Even though we focus on UV applications here, the results are applicable to longer wavelength such as visible and infrared, though lattice contributions to the dielectric behavior of these materials may need further study for a more accurate representation at wavelengths longer than the near infrared range.

## 4. Conclusion

We have investigated the refractive index of AlGaN, BAlN and BGaN alloys using hybrid density functional theory. The main goal is to design lattice-matched optical structures in the ultraviolet range. The AlGaN results were shown to reasonably match experimental reports. A peculiar behavior of the refractive indices of different boron alloys is found unlike other known nitrides. This unique behavior may be attributed to the electronic properties of the boron atom and the low slope of the refractive index of wurtzite BN. Our data is interpolated to fit different compositional needs, and could be used in designing a myriad of lattice-matched and lattice-mismatched heterostructures for photonic and optoelectronic devices. Structures made of these materials could benefit from the large range of refractive indices and refractive index differences for all wavelengths down to the deep UV range. A lattice-matched structure with a high difference in refractive index of $B_{0.108}Ga_{0.892}N$/AlN is

chosen as an example. It is used to demonstrate an optimized DBR at 375 nm having a peak reflectivity of 99.8% and a bandwidth of 26 nm with only 25 pairs. The number of pairs could be increased or decreased to tune the DBR's reflectivity. These results are useful for lattice matching and lattice engineering of UV compatible materials opening the door for different applications, including vertical emitters such as VCSELs.

## Acknowledgments

The authors acknowledge support of KAUST Baseline Fund BAS/1/1664-01-01, Competitive Research Grants URF/1/3437-01-01 and URF/1/3771-01-01, and GCC Research Council REP/1/3189-01-01.

## Data availability statement

All data that support the findings of this study are included within the article (and any supplementary files).

## ORCID iDs

Feras AlQatari https://orcid.org/0000-0001-7620-4569
Udo Schwingenschlögl https://orcid.org/0000-0003-4179-7231
Xiaohang Li https://orcid.org/0000-0002-4434-365X

## References

[1] Ambacher O 1998 *J. Phys. D: Appl. Phys.* **31** 2653
[2] Kim H M, Cho Y H, Lee H, Kim S I, Ryu S R, Kim D Y, Kang T W and Chung K S 2004 *Nano Lett* **4** 1059
[3] Ambacher O *et al* 1999 *J. Appl. Phys.* **85** 3222
[4] Oleg L, Pauporté T and Viana B 2010 *Adv. Mater.* **22** 3298
[5] Muramoto Y, Kimura M and Nouda S 2014 *Semicond. Sci. and Technol* **29** 084004
[6] Tadatomo K, Okagawa H, Ohuchi Y, Tsunekawa T, Imada Y, Kato M and Taguchi T 2001 *Jpn. J. Appl. Phys.* **40** L583
[7] Nishida T, Saito H and Kobayashi N 2001 *Appl. Phys. Lett.* **79** 711
[8] Iida K *et al* 2004 *Jpn. J. Appl. Phys.* **43** L499
[9] Yoshida H, Yamashita Y, Kuwabara M and Kan H 2008 *Appl. Phys. Lett.* **93** 241106
[10] Guo W *et al* 2018 *Adv. Funct. Mater.* **28** 1802395
[11] Lin R, Galan S V, Sun H, Hu Y, Alias M S, Janjua B, Ng T K, Ooi B S and Li X 2018 *Photon. Res.* **6** 124
[12] Li X *et al* 2015 *Appl. Phys. Lett.* **106** 041115
[13] Li X, Xie H, Ryou J H, Ponce F A, Detchprohm T and Dupuis R D 2015 *Appl. Phys. Lett.* **107** 241109
[14] Fisk P T H, Sellars M J, Lawn M A and Coles C 1997 *IEEE Trans. Sonics Ultrason. Ferroelectr. Freq. Control* **44** 344
[15] Zhao Y S, Hibbard D L, Lee H P, Ma K, So W and Liu H 2003 *J. Elect. Mater* **32** 1523
[16] Lin H Y *et al* 2015 *Optics Express* **23** A27
[17] Rattier M, Benisty H, Stanley R P, Carlin J F, Houdré R, Oesterle U, Smith C J M, Weisbuch C and Krauss T F 2002 *IEEE J. Select. Topics in Quantum Electron* **8** 238
[18] Sun H *et al* 2018 *Appl. Phys. Express* **11** 011001
[19] Liu Y S *et al* 2016 *Appl. Phys. Express* **9** 111002
[20] Mitrofanov O, Schmult S, Manfra M J, Siegrist T, Weimann N G, Sergent A M and Molnar R J 2006 *Appl. Phys. Lett.* **88** 171101
[21] Waldrip K E, Han J, Figiel J J, Zhou H, Makarona E and Nurmikko A V 2001 *Appl. Phys. Lett.* **78** 3205
[22] Perillat-Merceroz G, Cosendey G, Carlin J F, Butté R and Grandjean N 2013 *J. Appl. Phys.* **113** 063506
[23] Sadler T C, Kappers M J and Oliver R A 2009 *Phys. Status Solidi C* **6** S666
[24] Berger C, Dadgar A, Blasing J and Krost A 2013 *J. Crystal Growth* **370** 87
[25] Abid M *et al* 2012 *Appl. Phys. Lett.* **100** 051101
[26] Watanabe S, Takano T, Jinen K, Yamamoto J and Kawanishi H 2003 *Phys. Status Solidi C* **7** 2691
[27] Zhang M and Li X 2017 *Phys. Status Solidi B* **254** 1600749
[28] Said A, Debbichi M and Said M 2016 *Optik* **127** 9212
[29] Liu K, Sun H, AlQatari F, Guo W, Liu X, Li J, Castanedo C G T and Li X 2017 *Appl. Phys. Lett.* **111** 222106
[30] Sun H, Park Y, Li K-H, Castanedo C G T, Alowayed A S, Detchprohm T, Dupuis R D and Li X 2017 *Appl. Phys. Lett.* **111** 122106
[31] Li X, Wang S, Liu H, Ponce F A, Detchprohm T and Dupuis R D 2017 *Phys. Status Solidi B* **254** 1600699
[32] Turiansky M E, Shen J X, Wickramaratne D and Van de Walle C G 2019 *J. Appl. Phys.* **126** 095706
[33] Cramer C, English J, Bonef B and Speck J S 2019 *J. Vac. Sci. Technol. A* **37** 061502
[34] Tran T B, Liao C-H, AlQatari F and Li X 2020 *Appl. Phys. Lett.* **117** 082102
[35] Gunning B P, Moseley M W, Koleske D D, Allerman A A and Lee S R 2017 *J. Cryst. Growth* **464** 190
[36] Ougazzaden A, Gautier S, Moudakir T, Dhebbour Z, Lochner Z, Choi S, Kim H J, Ryou J H, Dupuis R D and Sirenko A A 2008 *Appl. Phys. Lett.* **93** 083118
[37] Yamashita M, Hamada N, Funashima H and Yoshiya M 2015 *Phys. Status Solidi C* **12** 647
[38] Paier J, Marsman M and Kresse G 2008 *Physical Review B* **78** 121201
[39] Takeuchi K, Adachi S and Ohtsuka K 2010 *J. Appl. Phys.* **107** 023306
[40] Muth J F, Brown J D, Johnson M A L, Yu Z, Kolbas R M, Cook J W and Schetzina J F 1999 *MRS Internet J. Nitride Semicond. Res.* **4** 502
[41] Kresse G and Furthmuller J 1996 *Phys. Rev. B* **45** 11169
[42] Kresse G and furthmuller J 1996 *Comp. Mater. Sci.* **6** 15

[43] Perdew J P, Ruzsinszky A, Csonka G I, Vydrov O A, Scuseria G E, Constantin L A, Zhou X and Burke K 2008 *Phys. Rev. Lett.* **100** 136406
[44] Edgar J H 1994 *Properties of Group III Nitrides* (London: INSPEC)
[45] Heyd J, Scuseria G E and Ernzerhof M 2006 *J. Chem. Phys.* **124** 219906
[46] Yang M, Chang B, Hao G, Wang H and Wang M 2015 *Optik* **126** 3357
[47] Djurisic A B, Chan Y and Li E H 2001 *Proc. SPIE* 4283, 630 Physics and Simulation of Optoelectronic Devices IX
[48] Tisch U, Meyler B, Katz O, Finkman E and Salzman J 2001 *J. Appl. Phys.* **89** 2676
[49] Smith J C, Pribram-Jones A and Burke K 2016 *Phys. Rev. B* **93** 245131
[50] Fox M 2001 *Optical Properties of Solids* (New York: Oxford University Press)
[51] Segura A, Cusco R, Taniguchi T, Watanabe K, Cassabois G, Gil B and Artus L 2019 *J. Phys. Chem. C* **123** 20167
[52] Liao C-H, AlQatari F and Li X 2020 *arXiv preprint* arXiv:2005.08274
[53] Xie D, Qiu Z R, Talwar D N, Liu Y, Song J-H, Huang J-L, Mei T, Liu C W and Fang Z C 2015 *Int. J. Nanotechnol* **12** 97
[54] Gautier S *et al* 2011 *Proc. SPIE* 7940Oxide-based Materials and Devices II, 79400X
[55] Li X *et al* 2015 *Phys. Status Solidi A* **212** 745
[56] Lyons J L, Janotti A and Van de Walle C G 2014 *Physical Review B* **89** 035204
[57] Akima H 1970 *J. Assoc. Comput. Mach.* **17** 589
[58] de Boor C 1978 *A Practical Guide to Splines* (NY, USA: Springer-Verlag)
[59] Hiraiwa K, Muranaga W, Iwayama S, Takeuchi T, Kamiyama S, Iwaya M and Akasaki I 2020 *Appl. Phys. Express* **13** 055506
[60] Liu Y-S *et al* 2016 *Appl. Phys. Lett.* **109** 081103
[61] Orfanidis S J 2016 *Electromagnetic Waves and Antennas* (NJ, USA: Rutgers University) eceweb1.rutgers.edu/~orfanidi/ewa/
[62] Honda T, Katsube A, Sakaguchi T, Koyama F and Iga K 1995 *Jpn. J. Appl. Phys.* **34** 3527
[63] Wang G-J, Hong G-S, Chen Y-Y, Yang Z-J, Tsai T-L, Lin Y-S and Lin C-F 2017 *Appl. Phys. Express* **10** 122102
[64] Mehta K *et al* 2018 *IEEE J. Quantum Electron* **54** 2400507
[65] Serkland D K, Peake G M, Geib K M, Lutwak R, Garvey R M, Varghese M and Mescher M 2006 *Proc. SPIE* 6132 Vertical-Cavity Surface-Emitting Lasers X, 613208
[66] Lumerical Inc (http://lumerical.com/tcad-products/fdtd/)